Conformational Properties and Entropic Partitioning of Topologically Complex Polymers under Confinement

Zhong Chen and Fernando A. Escobedo*

School of Chemical Engineering, Cornell University, Ithaca, New York 14850-5201

Received July 20, 2001; Revised Manuscript Received September 26, 2001

ABSTRACT: The effect of molecular topology on the properties of isolated polymer chains trapped in a repulsive slit was investigated using off-lattice Monte Carlo simulations. Three different chain architectures were studied: star-branched, dendritic, and hyperbranched chains. The linear dimensions of the polymer coil, the density profiles across the slit, and the confinement force F were obtained from the simulations and compared with those of linear chains. It is found that scaling theory for linear chains describes well all the properties examined of star molecules and the scaling of the linear dimensions of dendrimers and hyperbranched polymers. The relative partition coefficient at the dilution limit was estimated from the data of F vs slit separation D. It is shown that for very narrow D branched polymers tend to be depleted in the pore relative to linear chains with the same molecular weight; this trend is reversed, however, at large D.

1. Introduction

The conformational and thermodynamic properties of polymer chains are strongly affected by geometric confinement.[1,2] This phenomenon is relevant to numerous applications of polymers such as in chromatographic separations, colloidal stabilization, thin-film processing, and the preparation of clay-based nanocomposites.[3] Applications are being developed that exploit the thermodynamically driven partitioning of confined polymers. For example, the high osmotic pressure chromatography is intended for large-scale fractionation of polydisperse polymer solutions.[4] Entropically driven surface segregation of certain components in a confined polymer solution or melt could also be used to functionalize the surface of thin films.[5] From a fundamental standpoint, investigation of the properties of spatially confined polymers are also of great interest; e.g., a porous medium can be used as a probe to gauge the dimension of a polymer chain at different conditions,[6] and the study of wall-induced conformational changes in polymers may help us elucidate the activity of biopolymers near cell surfaces.[7]

While rigorous formulations exist for the configurational properties and partitioning of a Gaussian chain in pores,[8] a rigorous analytical theory has not been worked out for excluded-volume (EV) chains (a model adequate to describe good solvent conditions), and only approximate theories are available, e.g., mean field theory[9] and scaling theory.[10] Scaling theory has had the most general applicability so far, although it is valid for limiting conditions and can only give semiquantitative predictions.

Monte Carlo simulations have been used to simulate EV chains in pores. Simulations of a single athermal chain confined between flat, hard walls[11−13] have revealed that the chain dimensions (e.g., the end-to-end distance and the root-mean-square radius of gyration $R_g = \langle R_g^2 \rangle^{1/2}$) exhibit several regimes depending on the slit width D. The unconfined coil size is slightly reduced for large D. When the coil diameter is commensurate with D, i.e., $D \approx 2R_g$, the chain size is squeezed, reaching a minimum. For $D \ll R_g$ the chain is severely flattened to a pancake shape. The scaling of chain linear dimensions with D/R_g is found to be in good agreement with the scaling predictions in the narrow slit limit (i.e., $D \ll R_g$). The density profiles of the chain monomers across the slit and the confinement force have also been calculated and compared to theory. The effect of concentration on the size and partitioning of chains into a pore has been studied by on-lattice Monte Carlo simulations.[6] A weak-to-strong penetration transition is observed as the bulk concentration increases.[10,14] Off-lattice simulations have provided detailed information on the chain structure and density profiles near a surface for dense systems.[15−17] It was shown that chains are depleted near the walls at low densities but are enhanced at high densities and that chain ends and shorter chains tend to segregate near the wall (to gain conformational entropy).

Most of the theoretical and simulation work on confined polymers so far has been concerned with linear chains; studies on polymers with more complicated topology, such as rings, stars, dendrimers, and hyperbranched polymers (HBP), are very limited. It is well-known that polymers with complex internal architecture have quite different static and dynamic properties. The question then arises as to how the internal architecture affects the properties of confined polymer chains. Just as in the case of linear polymers, rigorous theoretical solutions are available for an ideal self-crossing cyclic chain confined in slitlike pores,[18] and scaling results are available for a cyclic EV chain.[19] These theories predict substantial differences in the partition coefficients of linear and cyclic macromolecules under weak adsorption conditions, opening up the possibility for the development of a new method for separating cyclic and linear polymers.[20] An on-lattice simulation study was carried out for the adsorption of polymer chains with different molecular architectures, including linear, star, and cyclic chains, on a solid surface.[21] For weakly adsorbed chains it was shown that ring polymers are adsorbed always ca. 50% more than linear and star-branched ones, while the properties of adsorbed linear and star polymers are very similar. To the best of our knowledge, no simulation has been reported on the properties of

10.1021/ma011283y CCC: $20.00
Published on Web 10/27/2001

topologically complex polymers confined in repulsive slit pores.

In this work, the properties of confined polymers with various topologies are investigated using Monte Carlo simulation. Model polymers employed include stars, dendrimers, and HBPs. Stars and dendrimers are among the most important regularly branched molecules. The topology of randomly branched HBPs, however, can vary significantly depending on the synthesis conditions. In this study, model HBPs are produced using a kinetic Monte Carlo scheme that has been implemented to simulate the formation of Pd−α-diimine-catalyzed polyethylene.[22] It has been shown experimentally that Pd-catalyzed polyethylene has a unique branch-on-branch topology that can be controlled by ethylene pressure.[23−26] The topology varies from predominantly linear polyethylene with many short branches at high pressures to a compact, densely branched HBP at low pressure. Our Monte Carlo scheme generates various branching topologies by mimicking the probabilistic nature of the chain-walking mechanism that has been proposed to explain this polymerization process. Such a system is an ideal candidate for fundamental computational studies aimed at elucidating the correlation between polymer topology and confined properties because it involves the simplest possible polymer type (polyethylene) and its branching topology can be readily controlled.

Geometric confinement is realized in this work by placing polymers inside a slit with hard walls separated by a distance D. We limit ourselves to the case of an isolated polymer chain with hard-sphere interaction sites, which corresponds to a dilute polymer solution in good solvent. Since no adsorption force is present in our system, the properties of polymers are solely determined by the interplay of two factors: (i) the entropy losses due to the slit walls restricting the set of possible conformations and (ii) the tendency of the chain to compensate such losses by preferentially adopting conformations that satisfy confinement and topological constraints. In our simulations, the linear dimension of polymers (e.g., the components of R_g), the density profile across the slit, and the mean repulsive force (F) were collected and analyzed within the context of scaling theory. It is found that the scaling behavior of star molecules is essentially identical to that of linear chains (for the number of arms f and chain lengths studied). For dendrimers and HBPs, the scaling of the linear dimensions is well described by the scaling theory of linear chains, but the density profiles and F deviate from the scaling predictions and the degree of deviation seems to depend on the monomer density inside the polymer coil. The relative partition coefficient K^* estimated from the F vs D data indicates that, for very short D, branched polymers tend to be depleted in the pore relative to linear chains of the same molecular weight. Such a trend is reversed at large D, where branched polymers tend to be concentrated in the pore. Likewise, differences in topology are shown to affect the relative partitioning of different branched polymers.

The rest of this paper is organized as follows. In section 2, we summarize relevant results from scaling theory for confined polymers. In section 3, we present the details of the Monte Carlo simulations. In section 4, we present the results of chain linear dimensions, density profiles, confinement forces, and partition coefficients for various polymer topologies. Finally, in section 5, we summarize the major results of this paper and provide a few concluding remarks.

2. Scaling Predictions

We consider a slit consisting of two parallel impenetrable walls a distance D apart. The coordinate system is set up such that the bottom wall is the xy-plane containing the origin. The z-axis is perpendicular to the walls and the top wall is thus at $z = D$ (see Figure 1a).

For an isolated linear chain confined in the slit, the component of the mean-square gyration radius parallel to the walls scales as[11,14]

$$R_{g||}^{\,2} = \frac{2}{3} R_{gb}^{\,2} \tilde{R}_{||}(D/R_{gb}) \tag{1}$$

where R_{gb}^2 is the mean-square radius of gyration in the bulk; $\tilde{R}_{||}$ is a universal scaling function. In the limit of narrow slits ($D/R_{gb} \ll 1$),

$$\tilde{R}_{||} = c_{||}(D/R_{gb})^{-\xi} \tag{2}$$

where $c_{||}$ is another universal constant and $\xi = 2(\nu_2 - \nu_3)/\nu_3$, where ν_2 and ν_3 are the values of the scaling exponent ν (as in $R_g \sim N^\nu$, where N is the number of monomers in the polymer chain) in two- and three-dimensional space, respectively. For a linear chain in good solvent, $\nu_2 = {}^3/_4$ and $\nu_3 \approx 0.59$.[10]

For a star molecule with f arms and N_b beads per arm, each arm can be seen as a series of spherical blobs.[27] For a star molecule in a good solvent

$$R_{gb} \sim N_b^{\,\nu_3} f^{\,(1-\nu_3)/2} \tag{3}$$

On the basis of the same "blob" picture, it can be shown that in a two-dimensional space

$$R_{gb} \sim N_b^{\,\nu_2} f^{\,(1-\nu_2)} \tag{4}$$

The values of ν_2 and ν_3 in eqs 3 and 4 are the same as those of linear chains. If the star molecule is confined in a slit, we can include f in the scaling relation by assuming that

$$R_{g||}^{\,2} = \frac{2}{3} R_{gb}^{\,2} \tilde{R}_{||}(D/R_{gb}) f^{\,m} \tag{5}$$

As D approaches the narrow-slit limit, the crossover to two-dimensional behavior must occur, at which point $\tilde{R}_{||}$ can be described by eq 2 and

$$m = (2\nu_3 - \nu_3\nu_2 - \nu_2)/\nu_3 \tag{6}$$

m is exactly zero if a value of ${}^3/_5$ is used for ν_3 and remains negligible even if the more accurate value of $\nu_3 = 0.59$ is used. Therefore, aside from the effect of f on the magnitude of R_{gb}, the scaling behavior of $R_{g||}^2$ for star chains is predicted to be independent of f. This result also implies that in the narrow-slit limit the linear dimensions of a confined star molecule obey the same scaling relations as those of a linear chain.

The scaling function $\tilde{R}_{||}$ for a dendrimer has the same form as that for a linear chain but with a different exponent ξ. Such a result follows by considering the dependence of $\tilde{R}_{||}$ on N while setting aside the dependence of R_{gb} on the separator length N_s (i.e., the number of bonds between branched points). It is unclear, however, what values for ν_3 and ν_2 should be used to

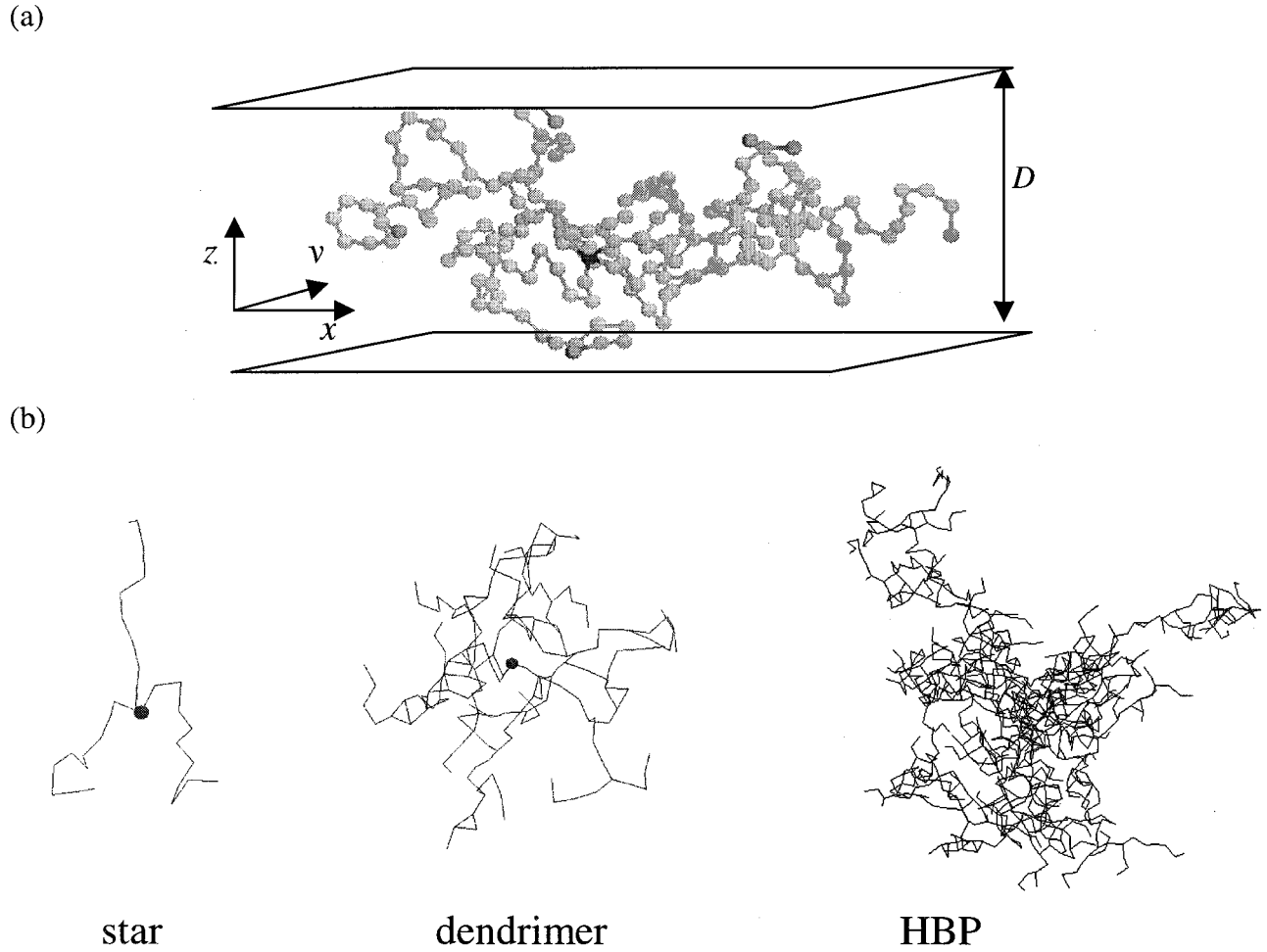

Figure 1. (a) Schematic representation of the model system. A star molecule with six arms is shown within the slit. (b) Sample snapshots of model polymers studied: star, dendrimer, and HBP; only the backbones are shown for clarity.

evaluate ξ. For example, for a dendrimer in a good solvent, a value of $^1/_5$ was obtained for ν_3 (i.e., $R_{gb} \sim N^{1/5}$) based on a theoretical calculation,[28] while a value close to $^1/_3$ was reported in a molecular simulation study.[29] No reference value for ν_2 is available for dendrimers.

For a single linear chain, the monomer density profile [$\rho(z)$] across the slit in the region near each wall (i.e., $z/R_{gb} \ll 1$) is predicted to scale as[10]

$$\rho(z) \sim z^{1/\nu_3} \tag{7}$$

In the narrow-slit limit, the confinement force F, which is defined as the derivative of the logarithm of the chain partition function with respect to the position of the wall in the z direction, is predicted to scale as[30]

$$F/k_BT \sim \frac{1}{D}(D/R_{gb})^{-1/\nu_3} \tag{8}$$

where k_B is Boltzmann's constant and T is the temperature. To the best of our knowledge, no scaling theory is available concerning $\rho(z)$ or F for topologically complex polymers under confinement.

3. Methodology

Model Systems. Polymers are modeled as strings of hard beads of uniform diameter σ (continuum space). This "athermal" molecular model is intended to describe a polymer molecule in a good "implicit" solvent; i.e., the preference of polymer sites to be surrounded by solvent rather than by other polymer sites gives rise to an effective repulsive interaction among polymer-sites. The bond length bl is allowed to fluctuate within the range [$0.85\sigma-1.15\sigma$], and no overlap is allowed between nonbonded spheres; this model can be seen as the continuum-space counterpart of the on-lattice bond fluctuation model commonly used in simulation work.[31] No long-range interactions or bond angle constraints are incorporated; in such a flexible coarse-grained model, each hard sphere represents several actual "mers" in a polymer. The simulation box is bounded by two hard walls perpendicular to the z direction. The walls are impenetrable to the centers of the sites; for a wall separation D (in units of σ), the sites can move across a distance $D - 1$ in the z direction.

Three different model molecules were employed in this study, namely stars, dendrimers, and HBPs. The star polymers employed have different structures, with $f = 3$, 6, and 10, respectively, and N_b ranging from 30 to 252. The dendrimers under study have a central core that branches off into three arms. Each arm branches into two additional branches. The generation number ranges from 3 to 7, and N_s has two different values, 4 and 12. HBPs are generated by a stochastic Monte Carlo model which mimics the formation of polyethylene molecules via the chain-walking mechanism.[22] The HBPs used in this work are such that $\nu_3 = 0.54$ (a value close to that reported experimentally:[26] $\nu_3 \sim 0.5$). The size of these model molecules ranged from $N = 181$ to

3061, and at least two different realizations for each N were simulated to obtain more representative statistics.

Conformational Properties. Hopping moves and pivot rotation were used to relax the chain conformation;[22] translational moves along the z direction were also implemented. After a preequilibration period, at least 2×10^7 production cycles were performed per state point; one MC move per site is attempted in each cycle. The production period was divided into 10 blocks for the purpose of statistical analysis. Error bars were typically smaller than the data marker and are not shown in the figures. R_g^2 and its component in the x, y ($R_{g||}^2$) directions were collected in the production period. The monomer density profile, $\rho(z)$, was obtained by dividing the region between the walls into 100 equal-sized bins and collecting the number of sites in each bin over the whole length of the production period. $\rho(z)$ represents average number of sites per bin normalized in such a way that

$$\int_0^D \rho(z)\, \mathrm{d}z = N \tag{9}$$

Confinement Force. The force exerted by the polymer chain on the walls is estimated from the change in the Helmholtz potential A when the wall separation is decreased from D to $D - \mathrm{d}D$,

$$F = -\left.\frac{\partial A}{\partial D}\right|_D \tag{10}$$

This derivative is evaluated using the virtual-parameter-variation method (VPV):[32]

$$F = -\left.\frac{\partial A}{\partial D}\right|_D = -\frac{1}{\beta}\lim_{\Delta D \to 0}\frac{\ln\langle \exp(-\beta \Delta U)\rangle}{\Delta D} \tag{11}$$

ΔU is the change of the configurational energy due to the separation change ΔD and $\beta = 1/k_B T$. After every MC cycle, a series of trial changes in slit separation ΔD were performed, and the corresponding values of $\exp(-\beta \Delta U)$ were calculated and recorded as a histogram with equal-sized bins. At the end of the simulation, the average values of $\exp(-\beta \Delta U)$ were plotted as a function of ΔD and extrapolated to $\Delta D = 0$. The extrapolation is done by linear regression of $\exp(-\beta \Delta U)$ on ΔD near $\Delta D = 0$. F can also be obtained from the relation between pressure and hard-wall contact density[33]

$$\beta F = \beta P \times (\text{area of the wall}) = \rho(0) \tag{12}$$

Note that according to eq 9 $\rho(0)$ has units of 1/(unit length). Equation 12 can be derived directly from eq 10 as outlined in ref 34. $\rho(0)$ can be estimated by extrapolating $\rho(z)$ near the wall to $z = 0$. Our simulations show that both methods generate essentially the same results for F; only the results from the VPV method are reported.

Pore-to-Bulk Partitioning Coefficient. From eq 10, it follows that the free energy change of moving isothermally an isolated polymer chain from a free, unconfined bulk environment to a slit with separation D is

$$\Delta A = -\int_\infty^D F(D')\, \mathrm{d}D' \tag{13}$$

However, since we are interested in the relative change of A with respect to a free, unconfined polymer coil, then such a contribution (F^0) should be deducted from F. The force of such an ideal system can be calculated from the ideal gas law, i.e., $\beta F^0 = 1/D$ (as confirmed by test simulations on a linear chain for $D \to \infty$ where $F \to F^0$). Thus

$$\Delta A = -\int_\infty^D (F - F^0)\, \mathrm{d}D' = -\int_\infty^D \left(F - \frac{1}{\beta D'}\right) \mathrm{d}D' \tag{14}$$

To determine the partition coefficient in the dilute solution limit, we consider the chemical potential of a single polymer chain, which is a function of the concentration c and pore separation D, i.e., $\mu = \mu(c,D)$:

$$\mu_{\text{pore}}(c_p,D) = \mu_{\text{intra}}(0,D) + \frac{1}{\beta}\ln c_p + \mu_{\text{inter}}(c_p,D) \tag{15}$$

$$\mu_{\text{bulk}}(c_b,\infty) = \mu_{\text{intra}}(0,\infty) + \frac{1}{\beta}\ln c_b + \mu_{\text{inter}}(c_b,\infty) \tag{16}$$

where subscript p denotes slit pore and b denotes bulk. μ_{inter} refers to the contribution from the intermolecular interactions, which is negligible in the dilute solution limit. μ_{intra} is the contribution from intramolecular interactions for a given D, including polymer−wall interactions. We can then write

$$\mu_{\text{intra}}(0,D) = \mu_{\text{intra}}(0,\infty) + \Delta A = \mu_{\text{intra}}(0,\infty) - \int_\infty^D \left(F - \frac{1}{\beta D'}\right) \mathrm{d}D' \tag{17}$$

Since at equilibrium $\mu_{\text{pore}} = \mu_{\text{bulk}}$, then from eqs 15−17 we can obtain the partition coefficient K^0:

$$\ln K^0 = \ln \frac{c_p}{c_b} = \beta \int_\infty^D \left(F - \frac{1}{\beta D'}\right) \mathrm{d}D' \tag{18}$$

For two polymers A and B with different topology but having the same (dilute) bulk concentration c_b, we can write

$$\ln K^* = \ln \frac{c_p^{\,A}}{c_p^{\,B}} = \beta \int_\infty^D (F^A - F^B)\, \mathrm{d}D' \tag{19}$$

Because μ of a linear chain in a slit pore can be readily obtained using Widom's test-particle insertion method,[35] the above integration scheme was tested by comparing K^0 data obtained from μ data and from F data. The chemical potentials of a 20-mer linear chain in the bulk [$\beta\mu_{\text{intra}}(0,\infty) = 9.457$] and in a slit with $D = 4$ [$\beta\mu_{\text{intra}}(0,4) = 6.785$] were measured using the configurational-bias particle-insertion method.[35] From eqs 17 and 18 it follows that $\ln K^0 = \ln[(c_p(D=4))/c_b] = \beta\mu_{\text{intra}}(0,\infty) - \beta\mu_{\text{intra}}(0,4) = -2.67$. From F vs D data ($4 \le D \le 40$) for a 20-mer, integration of eq 18 leads to $\ln K^0 = -2.73$. These results differ in ~2%, well within simulation data error bars. As a further test, K^* for two linear molecules (A: 20-mer; B: 30-mer) at $D = 4$ was also obtained; we found $\ln K^* = 1.55$ from the μ-approach and 1.52 from the F-approach (eq 19); once again, the difference is ~2%. The F-approach should be more practical than the μ-approach for obtaining extensive K vs D data for large, topologically complex molecules.

4. Results and Discussions

A. Chain Linear Dimensions. The scaling behavior of $R_{g||}^2$ for star molecules confined in slits is shown in Figure 2 as a log−log plot of $^3/_2 R_{g||}^2/R_{gb}^2$ vs D/R_{gb}. The

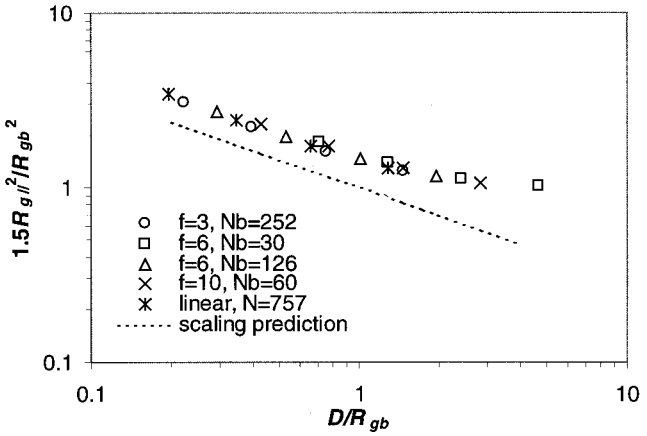

Figure 2. Normalized parallel component of the mean-square radius of gyration, $^3/_2R_{g||}^2/R_{gb}^2$, vs the relative separation D/R_{gb} for star molecules with different f and N_b. A linear chain is also shown for comparison. Dotted straight line indicates the slope of the scaling function for small D/R_{gb}, namely $-2(\nu_2 - \nu_3)/\nu_3$.

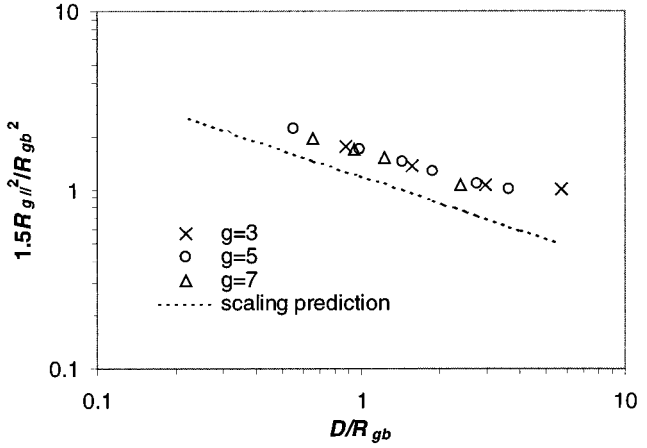

Figure 3. Same as Figure 2 but for dendrimers with $N_s = 4$ and varying generation numbers.

length of the arm (N_b) ranged from 30 to 252, and three different functionalities were studied, namely, $f = 3$, 6, and 10. It is observed in Figure 2 that all these curves, regardless of the value of f, collapse well into one master curve. When the slit separation is small ($D/R_{gb} < 1$ as in the figure), the scaling behavior of $\tilde{R}_{||}$ follows a trend consistent with the theoretical prediction stated in section 2. The theoretical scaling exponent, $\xi = 2(\nu_2 - \nu_3)/\nu_3 = 0.54$, is the slope of the straight line appearing in Figure 2. The scaling behavior of a linear chain with $N = 757$ is also plotted for comparison; as expected, it is indistinguishable from that of the star molecules (note that a linear chain of length N can be seen as a star molecule with $f = 2$ and $N_b = N/2$).

The results for dendrimers are given in Figure 3. The dendrimers studied have a uniform separator length (N_s) of 4. The generation number (g) ranges from 3 to 7. The scaling of R_{gb} with N in the bulk was first investigated, and a value of $\nu_3 = 0.32$ was obtained, which is consistent with reported molecular dynamics results.[31] If we assume that a dendrimer behaves as a two-dimensional object when it is confined to the narrowest slit ($D = 5$), then the value of ν_2 can be estimated from the scaling of $R_{g||}$ with N. From data of dendrimers with g from 3 to 5, a value of $\nu_2 = 0.4$ was obtained. It then follows that ξ in eq 2 is 0.5 for dendrimers; this exponent is shown in Figure 3 as the slope of the dotted straight line. These results show that scaling theory can predict the behavior of $R_{g||}$ for dendrimers in the narrow-slit limit when appropriate values for ν_2 and ν_3 are used.

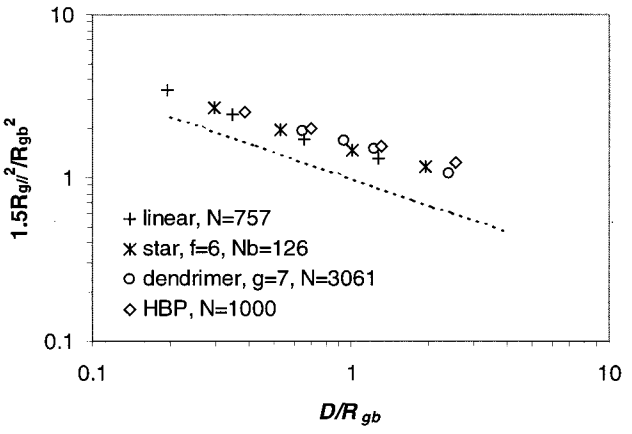

Figure 4. Scaling plot for linear dimension, $^3/_2R_{g||}^2/R_{gb}^2$ vs D/R_{gb} for isolated linear chains, stars, dendrimers, and HBPs.

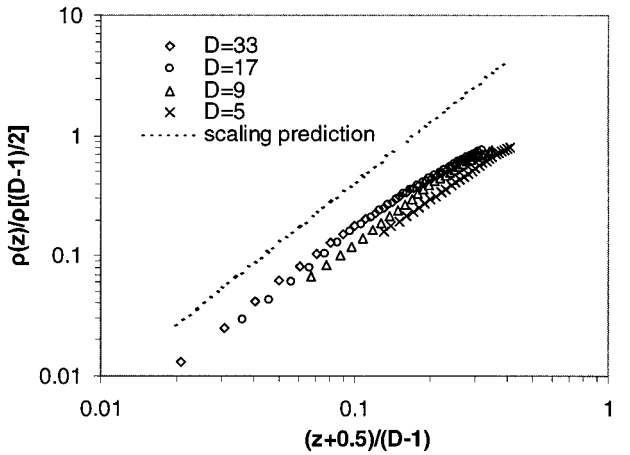

Figure 5. Density profiles $\rho(z)$, normalized by the density $\rho[(D - 1)/2]$ at the center of the slit, for a star molecule with $f = 6$, $N_b = 126$. The extrapolation length adopted is $\lambda = 0.5$. The dotted straight line indicates the predicted slope $1/\nu_3$ for a linear chain.

Figure 4 shows the scaling relation $^3/_2R_{g||}^2/R_{gb}^2$ vs D/R_{gb} for different molecular architectures. It is noted that the values of ξ for stars and linear chains (0.54) are very close to that of dendrimers (0.5). Also shown in Figure 4 is the scaling behavior of a HBP. Even though HBPs and dendrimers have very different molecular architectures, the scaling behavior of their linear dimensions is similar.

B. Density Profiles. The density profiles for a star molecule with $f = 6$, $N_b = 126$ are shown in Figure 5. $\rho(z)$ is shown reduced by $\rho[(D - 1)/2]$, the density at the center of the slit. An extrapolation length λ is introduced to replace $z^{1/\nu}$ in eq 7 by $(z + \lambda)^{1/\nu}$ to correct for the effect of bead size;[11] λ is set to be 0.5 (one-half σ). Since the hard wall is impenetrable to the center of the sites, a site located at $z = 0$ should actually be $\sigma/2$ away from the slit wall; this correction is unnecessary when $\lambda \ll z \ll R_{gb}$. In Figure 5, the dotted straight line depicts the predicted slope $1/\nu_3$ for a linear chain. It can be seen that in the region near the wall the linear-chain scaling prediction (eq 7) satisfactorily describes the behavior of the density profiles of star molecules.

The density profiles for a dendrimer with $g = 5$, $N_s = 4$ is illustrated in Figure 6. If the same value 0.5 is used for λ, $\rho(z)$ vs $(z + \lambda)$ does not follow the power law

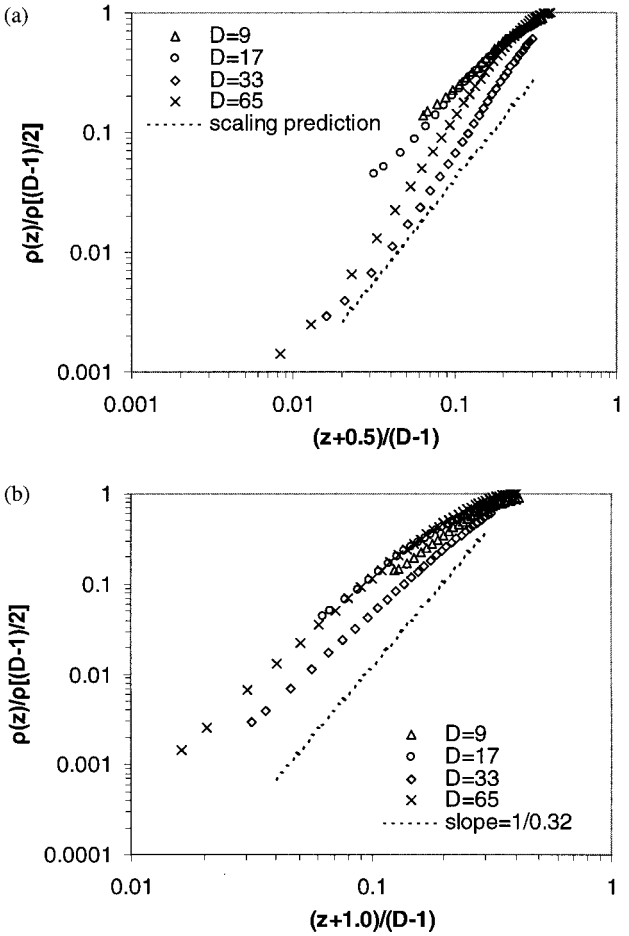

Figure 6. (a) Same as Figure 5 but for a dendrimer with $g = 5$, $N_s = 4$. (b). Same as (a) but with $\lambda = 1.0$. The dotted straight line indicates the slope $1/\nu_3$ where the value of ν_3 for a dendrimer (0.32) is used.

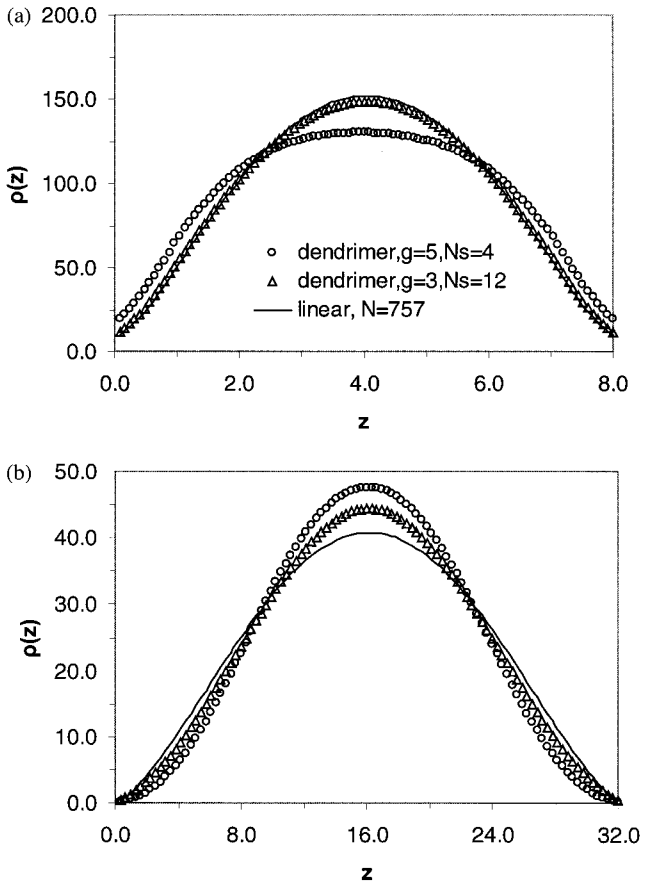

Figure 7. Density profiles $\rho(z)$ vs z for dendrimers with different N_s in a slit with separation (a) $D = 9\sigma$ and (b) $D = 33\sigma$.

relation given by eq 7 (i.e., a linear portion at small z is not seen in Figure 6a). To recover such a power law relation, λ needs to be increased to about 1 (see Figure 6b). In that case, an exponent 2.4 is obtained from the density profile at the largest slit separation $D = 65$, which is between the values of $1/\nu_3$ for linear chains (1.69) and dendrimers (3.1). This disparity in the behavior of $\rho(z)$ between dendrimers and linear chains may be due to the topology-induced rigidity of the dendrimer molecule studied. With such a short separator length (four), the monomers tend to become crowded at the outer shell of the molecular coil. Because the site density distribution inside a dendrimer affects $\rho(z)$, more rigid and topologically constrained molecules (with respect to a linear chain) are expected to exhibit larger departures from the linear-chain behavior for $\rho(z)$. This idea is validated in Figure 7 where the density profile of a dendrimer with $N_s = 12$ is plotted together with those of a dendrimer with $N_s = 4$ and a linear chain. A larger separation length renders the $N_s = 12$ dendrimer more flexible, and thus its ρ-profile is closer to that of a linear chain, especially at $D = 9$. As for the difference in λ between linear chains and dendrimers, it can be argued that a more meaningful interpretation of λ is that of being half of the persistence length (the "rigid" segments in the molecule). For a flexible linear chain, it is just half of the diameter of monomers. For the topologically constrained dendrimer (with $N_s = 4$), a rigid segment would contain more than one monomer and thus $\lambda > 0.5$. For the more flexible dendrimer with $N_s = 12$, satisfactory power law relations between $\rho(z)$ and $(z + \lambda)$ are observed in the region near the wall just using $\lambda = 0.5$ (results not shown).

In narrow slits (e.g., $D = 9$), the density in the vicinity of the walls [including $\rho(0)$] for the dendrimer with $N_s = 4$ is higher than that for the linear chain. This trend is reversed, however, in wider slits (e.g., $D = 33$). A similar behavior is also observed for the dendrimer with $N_s = 12$, though the differences are less significant. An insight into the deformation forces acting on a molecule is provided by the distribution of chain ends inside a slit. Figure 8 shows the density profiles of chain-ends and of inner-segments for a dendrimer with $g = 5$, $N_s = 4$ at slit separations $D = 9$ and 65, respectively. For large D (e.g., $D = 65$), the two density profiles are almost identical. In a narrow slit (e.g., $D = 9$), however, chain ends tend to be concentrated near the walls relative to inner segments. Similar graphs for linear, star, HBP (results not shown) indicate that as D decreases, the density at contact of chain ends always increase more than that for inner segments, but the effect is the mildest for linear chains and the strongest for dendrimers. This behavior evidences that an entropic gain ensues in having chain ends near the wall.

From the density profiles of HBPs with $N = 757$, 1000, and 2000 we find that $\lambda \sim 0.7$, which suggests that the rigidity of the HBPs lies between those of linear chains and dendrimers with $N_s = 4$. This result is consistent with the fact that ν_3 for these HBPs (0.54) lies between those for linear chains (0.59) and dendrimers (0.32); the value of ν_3 is in some sense a measure of the degree of branching in polymers.[22] An average

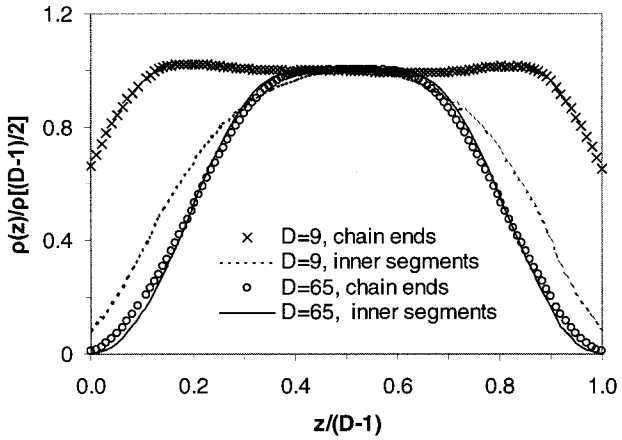

Figure 8. Density profiles of chain ends and inner segments for a dendrimer with $g = 5$, $N_s = 4$ for slit separations $D = 9$ and 65, respectively. The profiles are normalized so that they are unity at the center of the slit.

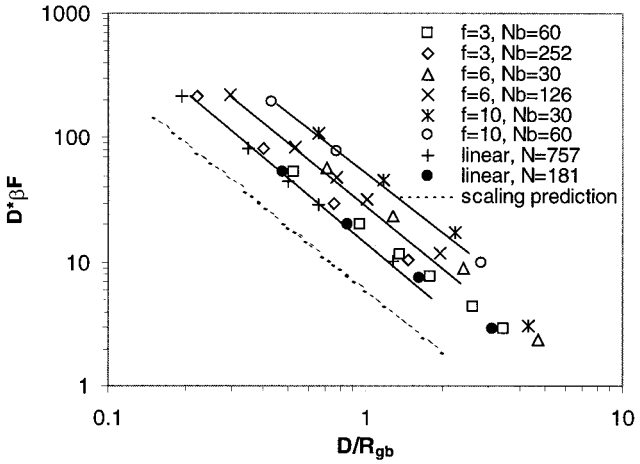

Figure 9. Scaling plot for the confinement force, DF vs D/R_{gb} for star molecules. Results for linear chains and the scaling prediction (dotted line) are also shown for comparison. The solid lines are drawn to guide the eye.

exponent of ca. 1.9 is obtained from $\rho(z)$of HBPs in a wider slit (e.g., with $D = 17$ and 33), which is quite close to $1/\nu_3$ if the value of ν_3 for these HBPs is used.

C. Confinement Force. The scaling of the confinement force (F) for star molecules is presented in Figure 9 as DF vs D/R_{gb} in a log−log plot. The results for a linear chain and the scaling prediction (eq 8) are also shown for comparison. The data points for stars can be readily classified into three groups according to the value of f, as indicated by three solid straight lines for $f = 3$, 6, and 10. Once again, the slopes of these three lines are very close to that of the linear chain, i.e., $-1/\nu_3$. For the star molecules studied, it can be concluded that the confinement force obeys the same scaling relation as that of linear chains but with an f-dependent scaling prefactor. Since the magnitude of R_{gb} also depends on f, this effect could be partially responsible for the variability of the scaling prefactor. To test this idea, DF is plotted vs D in Figure 11. It is seen that, in fact, linear and star molecules, with the same N and regardless of f, exert almost the same force when confined in the same slit.

The scaling of F for dendrimers with different structures is shown in Figure 10. In contrast to linear chains and stars, it is not clear whether a limiting power law relation exists between F and D/R_{gb} (see eq 8) for the

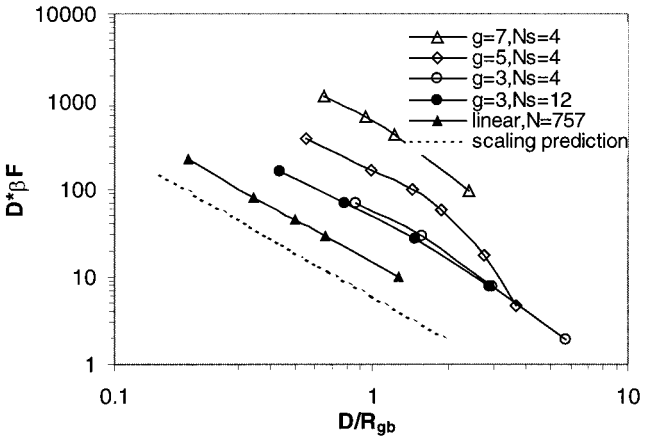

Figure 10. Same as Figure 9 but for dendrimers.

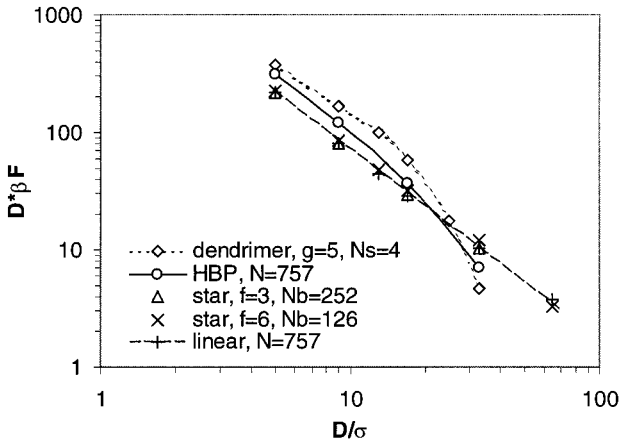

Figure 11. Scaling plot for the confinement force, DF vs D for linear chains, stars, dendrimers, and HBP with the same N (757). Lines are drawn to guide the eye.

narrow slit limit (at least for dendrimers with $N_s = 4$). If we assume that a region for small D/R_{gb} exists where a power law relation is valid, then the resulting exponent (e.g., ca. −1.4 for $g = 5$) is smaller than that for the linear chain (−1.69) and far different from what would be expected for a dendrimer based on the naive conjecture $-1/\nu_3 = -3.1$. It seems that because the average *mer* density inside the dendrimer tends to be high (and even grow with N), scaling theory is unable to satisfactorily describe the confinement behavior. The situation is similar for HBPs, where no clear scaling relation for F is found either (results not shown).

Figure 11 compares F for molecules with the same N but with different architectures. In narrow slits, F for dendrimers is larger than that for linear chains, but it decreases faster as D increases and eventually becomes smaller than F for linear chains for wide slits. Since F and $\rho(0)$ are related, this result is consistent with the fact that $\rho(0)$ for dendrimers is greater (smaller) than that of linear chains in a narrow (wide) slit. Further, it follows from Figure 8 that chain-end wall segregation must strongly affect F. The scaling of F for HBPs (relative to linear chains) is similar to that of dendrimers. Although star and linear chains have almost the same F, close inspection reveals that F for stars is also slightly larger for narrow slits and smaller for wide slits relative to linear chains.

D. Partition Coefficient. K^* from eq 19 provides a direct measure of the relative depletion within the pore of two polymers with different topology but having the

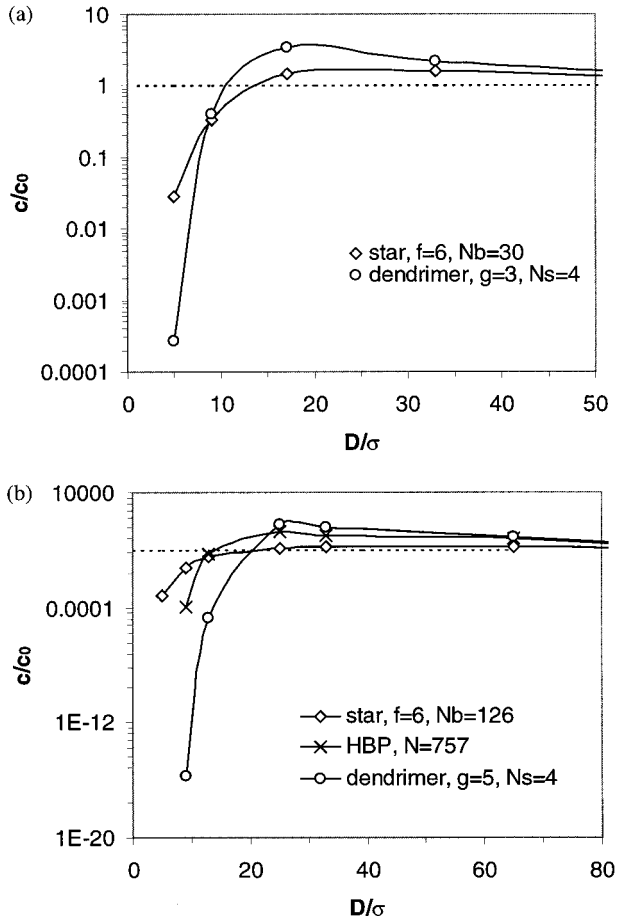

Figure 12. Intraslit relative partition coefficient at the dilution limit of stars, HBPs, and dendrimers with respect to linear chains of the same molecular weight; the bulk concentration is assumed to be the same for all molecules. (a) $N = 181$; (b) $N = 757$.

same (dilute) bulk concentration. Figure 12a shows some sample results for short polymers ($N = 181$) using a linear chain as reference ($c_p^B = c_0$ for the linear chain and $c_p^A = c$ for the branched chain). The values of F for polymers in slits with D ranging from 5 to 65 were obtained from simulations and the integration in that range was done numerically. Since $F \rightarrow 1/\beta D$ for $D \rightarrow \infty$, the value of F for $D > 65$ was estimated by assuming that $F = 1/\beta D + a/\beta D^2$, where parameter a was found from the value of F at $D = 65$. As expected, for large D, $K^* = c/c_0 \rightarrow 1$ regardless of topology. At very short separation, branched molecules tend to be depleted in the pore relative to linear chains. This is due to the fact that branched chains tend to have a higher average monomer concentration inside the polymer coil and experience a larger entropic penalty than linear chains upon strong confinement. However, this relative depletion of branched chains only ensues for $D < D_c$, where D_c is a crossover value where $K^* = 1$. For $D > D_c$ branched chains tend to be concentrated relative to linear chains; this can be explained by the smaller size of the branched chain coils. This argument is supported by the observation that the values of D_c are commensurate to $2R_{gb}$ for the branched molecules ($R_{gb} = 7.0$ for the star and 5.7 for the dendrimer). Note that, for $D > D_c$, K^* goes through a maximum and then plateaus to $K^* \rightarrow 1$. Similar trends are observed, and analogous arguments can be made if one were to compare stars and dendrimers. Dendrimers are depleted in the pore with respect to star molecules for some range of narrow D and reverse this trend elsewhere. Qualitatively similar results have been obtained for larger dendrimers, HBPs, and stars ($N = 757$) and are shown in Figure 12b. Note that just as with the results for $\rho(z)$ and F, the partitioning curve for HBPs appears to lie in between those for stars and dendrimers.

5. Conclusions

In this paper, the properties of topologically complex polymers in a spatially confined environment have been studied. The geometrical confinement is introduced by placing an isolated polymer chain inside a slit that consists of two parallel hard walls. Three different chain architectures were studied: star-branched, dendritic, and hyperbranched chains. The coil linear dimensions, the density profiles across the slit, and the confinement force F were obtained from the simulations and analyzed in the context of scaling theory. It was found that the scaling behavior of the coil linear dimensions is not sensitive to molecular topology; e.g., the scaling of $R_{g||}$ with D/R_{gb} exhibits almost identical behavior for all the molecular topologies employed. While the scaling behavior of the density profiles and confinement force for stars is analogous to that of linear chain, that is not the case for dendrimers and HBPs.

The partition coefficient K^* at the dilution limit has been estimated from the data of F vs D. It was shown that for very short D branched polymers tend to be depleted in the pore relative to linear chains; this trend is reversed for large D, where branched polymers tend to be concentrated in the pore and K^* passes through a maximum. These results suggest that the simulation approach used in this work could be used to predict the optimal size (and geometry) of porous media to perform entropic topology-based partitioning of polymers in solution. Simulations on the adsorption of topologically complex polymer will also be illuminating, especially in the adsorption critical regime where the energy gain due to adsorption compensates the entropy loss due to the confinement. Under those conditions, it is expected that chain topology will have a major impact on the partitioning of polymer solutions. By sequentially studying entropic and energetic effects, the role of molecular topology on the partition coefficient can be understood more clearly and may lead to new applications in the technology of polymer fractionation.

Acknowledgment. This work was supported by the National Science Foundation, Grant CTS-0081138, and by the ACS Petroleum Research Fund.

References and Notes

(1) Gorbunov, A. A.; Skvortsov, A. M. *Adv. Colloid Interface Sci.* **1995**, *62*, 31.
(2) Teraoka, I. *Prog. Polym. Sci.* **1996**, *21*, 89.
(3) Hackett, E.; Manias, E.; Gianelis, E. P. *Chem. Mater.* **2000**, *12*, 2161.
(4) Luo, M.; Teraoka, I. *Macromolecules* **1996**, *29*, 4226.
(5) Lee, H.; Archer, L. A. Functionalizing surfaces by field induced migration of copolymer additives. *Macromolecules*, in press.
(6) Wang, Y.; Teraoka, I. *Macromolecules* **1997**, *30*, 8473.
(7) Ito, Y. In *Synthesis of Biocomposite Materials*; Imanishi, Y., Ed.; Chemical Rubber: Boca Raton, FL, 1992; p 15.
(8) Cassaca, E. F. *J. Polym. Sci., Polym. Lett. Ed* **1967**, *5*, 773.
(9) Turban, L. *J. Phys. (Paris)* **1984**, *45*, 347.
(10) de Gennes, P.-G. *Scaling Concepts in Polymer Physics*; Cornell University Press: Ithaca, NY, 1979.
(11) Milchev, A.; Binder, K. *Eur. Phys. J. B* **1998**, *3*, 477.
(12) Cifra, P.; Bleha, T. *Macromol. Theory Simul.* **1999**, *8*, 603.

(13) de Joannis, J.; Jimenez, J.; Rajagopalan, R.; Bitsanis, I. *Europhys. Lett.* **2000**, *51*, 41.
(14) Daoud, M.; de Gennes, P.-G. *J. Phys. (Paris)* **1977**, *38*, 85.
(15) Kumar, S. K.; Vacatello, M.; Yoon, D. Y. *Macromolecules* **1990**, *23*, 2189.
(16) Yethiraj, A.; Hall, C. K. *Macromolecules* **1990**, *23*, 1865.
(17) Yethiraj, A.; Kumar, S.; Hariharan, A.; Schweizer, K. S. *J. Chem. Phys.* **1994**, *100*, 4691.
(18) Gorbunov, A. A.; Skvortsov, A. M. *Vysokomol. Soed. A* **1987**, *29*, 926.
(19) Skvortsov, A. M.; Gorbunov, A. A. *Vysokomol. Soed., A* **1986**, *28*, 1686.
(20) Skvortsov, A. M.; Gorbunov, A. A. *J. Chromatogr.* **1990**, *507*, 487.
(21) Sikorski, A. *Macromol. Theory Simul.* **2001**, *10*, 38.
(22) Chen, Z.; Escobedo, F. A., submitted to *Macromol. Theory Simul.*
(23) Johnson, L. K.; Killian, C. M.; Brookhart, M. *J. Am. Chem. Soc.* **1995**, *117*, 6414.
(24) Guan, Z.; Cotts, P. M.; McCord, E. F. *Polym. Prepr. (Am. Chem. Soc., Div. Polym. Chem.)* **1998**, *39* (2), 402.
(25) Guan, Z.; Cotts, P. M.; McCord, E. F.; McLain, S. J. *Science* **1999**, *283*, 2059.
(26) Cotts, P. M.; Guan, Z.; McCord, E.; McLain, S. *Macromolecules* **2000**, *33*, 6945.
(27) Daoud, M.; Cotton, J. P. *J. Phys. (Paris)* **1982**, *43*, 531.
(28) de Gennes, P.-G.; Hervet, H. *J. Phys., Lett.* **1983**, *44*, L351.
(29) Murat, M.; Grest, G. S. *Macromolecules* **1996**, *29*, 1278.
(30) Eisenriegler, E. *Phys. Rev. E* **1997**, *55*, 3116.
(31) Carmesin, I.; Kremer, K. *Macromolecules* **1988**, *21*, 2819.
(32) Vörtler, H. L.; Smith, W. R. *J. Chem. Phys.* **2000**, *112*, 5168.
(33) Percus, J. K. *J. Stat. Phys.* **1976**, *15*, 423.
(34) Dickman, R.; Hall, C. K. *J. Chem. Phys.* **1988**, *89*, 3168.
(35) Frenkel, D.; Smit, B. *Understanding Molecular Simulation*; Academic: San Diego, 1996.

MA011283Y